Preparation, Characterization, and Luminescence Properties of a 58-Electron Linear Pt_4 Cluster, $[Pt_4(dmb)_4(PPh_3)_2]^{2+}$ (dmb = 1,8-Diisocyano-*p*-menthane), and Its Diphosphine Polymers

Tianle Zhang, Marc Drouin, and Pierre D. Harvey*

Département de chimie, Université de Sherbrooke, Sherbrooke, Québec J1K 2R1, Canada

Received July 9, 1998

The title compounds $[Pt_4(dmb)_4(PPh_3)_2]Cl_2$ (**1**) and $\{[Pt_4(dmb)_4(diphos)]Cl_2\}_n$ (diphos = dppb (**2**), dppp (**3**), dpph (**4**)) have been prepared in good yields from the reaction of $Pt_2(dba)_3{\cdot}CHCl_3$ with 2 equiv of dmb and 1 equiv of PPh_3 for **1** (dba = dibenzylideneacetone) and from the reactions of $Pt_2(dba)_3{\cdot}CHCl_3$ with 2 equiv of dmb and 0.5 equiv of diphos for **2**−**4**. The structure for **1** consists of a quasi-linear $Pt_4L_2^{2+}$ species (L = PPh_3; d(PtPt) = 2.666(2), 2.655(2), 2.641(2) Å), where the dmb ligands bridge the Pt atoms forming a catenate. From Raman spectroscopy, the two ν(PtPt) active modes for **1** are observed at 162 and 84 cm^{-1} (F(PtPt) = 2.36 mdyn $Å^{-1}$). For **2**−**4**, the diphos ligands induce the formation of amorphous polymeric materials (X-ray powder diffraction patterns) with MW ranging from 84 000 to 307 000 according to viscometry. EHMO calculations predict that the HOMO and LUMO are the two dσ* orbitals arising from four interacting Pt atoms via the $d_{x^2-y^2}$, d_{z^2}, s, and p_x M atomic orbitals. These are mixed with the dδ and CNR(π*) MO's. From the examination of the position, absorptivity, and fwhm (full width at half maximum) of the strongly allowed low-energy UV−vis band, a dσ* → dσ* assignment is made (λ_{max} = 405 nm, ϵ = 35 800 M^{-1} cm^{-1}; EtOH for **1**). The four compounds are luminescent at 77 K in EtOH, where λ_{emi} are 750, 736, 750, and 755 nm and τ_e are 2.71, 4.78, 5.15, and 5.17 ns for **1**−**4**, respectively. On the basis of the Stokes shifts (10 000−12 000 cm^{-1}) and the long emission lifetimes, a phosphorescence dσ* → dσ* assignment is made for the observed emissions. Crystal data for **1**: crystal system triclinic; space group $P\bar{1}$; a = 12.624(4) Å; b = 14.24(2) Å; c = 27.312(3) Å; α = 92.35(3)°; β = 91.655(15)°; γ = 90.28(5)°; V = 4903(7) $Å^3$; Z = 2; D_{calc} = 1.528 g cm^{-3}; R_1 = 0.0738; wR_2 = 0.2097; S = 1.018.

Introduction

The preparation of linear Pt_4 species has been the topic of longstanding interest,[1] and their chemistry has been dominated by the so-called "platinum blue" complexes. However, the cluster valence electron count (CVE) is limited to only three counts: 62, 63, and 64 electrons, with formal Pt oxidation states of 2.00, 2.25, and 2.50, respectively. Examples where the Pt oxidation states are 2.14 and 2.37 also exist.[1h,i] More recently, this chemistry has been expanded to Pt_8 compounds,[2] and mixed-metal $M_2M'_2$ linear species (M = Pd, Pt; M′ = Cr, Mo).[1b,3] To our knowledge, there are no examples of Pt_4 species where the formal oxidation state is <2. We now wish to report the first example of a Pt_4 species with a 58-electron CVE where the Pt oxidation state is 0.5, using the bridging ligand dmb ($Pt_4(dmb)_4(PPh_3)_2^{2+}$). Although the dmb ligand is well-known for bridging M atoms separated by 2.7−5.3 Å,[4] there is no precedent where a catenate structure is formed with dmb, a property that is rare in inorganic chemistry. Finally, we wish to expand this chemistry to the preparation of new polymeric materials, in particular, block copolymers of the type $\{Pt_4(P\text{-}P)\}_n$, where P-P is $Ph_2P(CH_2)_nPPh_2$ (n = 4, 5, 6). These species are found to be luminescent at 77 K, and some spectroscopic properties are reported.

Experimental Section

Materials. K_2PtCl_4 (Pressure Chemical), $Ph_2P(CH_2)_nPPh_2$ (n = 4 (dppb), 5 (dppp), 6 (dpph)), and PPh_3 (Aldrich) were used without further purification. The phosphine purity was checked by ^{31}P NMR spectroscopy, and only a very small amount of phosphine oxide was detected (<1%). $Pt_2(dba)_3{\cdot}CHCl_3$[5] and dmb[6] were prepared according to standard procedures. All experiments were carried out under a N_2

* To whom correspondence should be addressed. Tel: (819) 821-8000, ext 2005. Fax (819) 821-8017. E-mail: pharvey@courrier.usherb.ca.

(1) (a)Matsumoto, K.; Matsunami, J.; Urata, H. *Chem. Lett.* **1993**, 597. (b) Matsumoto, K.; Urata, H. *Chem. Lett.* **1993**, 1061. (c) Matsumoto, K.; Miyamae, H.; Moriyama, H. *Inorg. Chem.* **1989**, *28*, 2959. (d) O'Halloran, T. V.; Mascharak, P. K.; Williams, I. D.; Roberts, M. M.; Lippard, S. J. *Inorg. Chem.* **1987**, *26*, 1261. (e) Bernardinelli, G.; Castan, P.; Soules, R. *Inorg. Chim. Acta* **1986**, *120*, 205. (f) Laurent, J.-P.; Lepage, P.; Dahan, F. *J. Am. Chem. Soc.* **1982**, *104*, 7335. (g) O'Halloran, T. V.; Roberts, M. M.; Lippard, S. J. *J. Am. Chem. Soc.* **1984**, *106*, 6427. (h) Matsumoto, K.; Takahashi, H.; Fuwa, K. *J. Am. Chem. Soc.* **1984**, *106*, 2049. (i) Matsumoto, K. *Bull. Chem. Soc. Jpn.* **1985**, *58*, 651. (j) Matsumoto, K.; Fuwa, K. *Chem. Lett.* **1984**, 569. (k) Hollis, L. S.; Lippard, S. J. *Inorg. Chem.* **1983**, *22*, 2600. (l) Hollis, L. S.; Lippard, S. J. *J. Am. Chem. Soc.* **1983**, *105*, 3494. (m) Matsumoto, K.; Takahashi, H.; Fuwa, K. *Inorg. Chem.* **1983**, *22*, 4086. (n) Matsumoto, K.; Fuwa, K. *J. Am. Chem. Soc.* **1982**, *104*, 898. (o) Hollis, L. S.; Lippard, S. J. *J. Am. Chem. Soc.* **1981**, *103*, 1232. (p) Barton, J. K.; Szalda, D. J.; Rabinowitz, H. N.; Waszczak, J. V.; Lippard, S. J. *J. Am. Chem. Soc.* **1979**, *101*, 1434. (q) Barton, J. K.; Rabinowitz, H. N.; Szalda, D. J.; Lippard, S. J. *J. Am. Chem. Soc.* **1977**, *99*, 2827. (r) Barton, J. K.; Caravana, C.; Lippard, S. J. *J. Am. Chem. Soc.* **1979**, *101*, 7269. (s) Mascharak, P. K.; Williams, I. D.; Lippard, S. J. *J. Am. Chem. Soc.* **1984**, *106*, 6428. (t) Yamamoto, Y.; Takahashi, K.; Yamazaki, H. *J. Am. Chem. Soc.* **1986**, *108*, 2458.

(2) (a) Matsumoto, K.; Sakai, K.; Nishio, K.; Tokisue, Y.; Ito, R.; Nishide, T.; Shichi, Y. *J. Am. Chem. Soc.* **1992**, *114*, 8110. (b) Sakai, K.; Katsumoto, K.; Nishio, K. *Chem. Lett.* **1991**, 1081. (c) Sakai, K.; Katsumoto, K. *J. Am. Chem. Soc.* **1989**, *111*, 3074.

(3) (a)Mashima, K.; Tanaka, M.; Tani, K. *J. Am. Chem. Soc.* **1997**, *119*, 4307. (b) Mashima, K.; Nakano, H.; Nakamura, A. *J. Am. Chem. Soc.* **1996**, *118*, 9083. (c) Mashima, K.; Nakano, H.; Nakamura, A. *J. Am. Chem. Soc.* **1993**, *115*, 11632.

10.1021/ic9807947 CCC: $18.00
Published on Web 02/17/1999

atmosphere. Solvents for spectroscopic measurements were purified according to procedures outlined in ref 7. The preparation of $Ag_2(dmb)_2(NO_3)_2$ will be reported elsewhere, but this compound was used here for comparison purposes. The $\{[Cu(dmb)_2]BF_4\}_n$ polymer with a MW of ~160 000 was prepared from a procedure outlined in ref 4c.

$[Pt_4(dmb)_4(PPh_3)_2]Cl_2$ (1). To a slurry solution containing 32.0 mg (0.0264 mmol) of $Pt_2(dba)_3{\cdot}CHCl_3$ in 10 mL of acetone was added 5 mL of a CH_2Cl_2 solution containing 34.0 mg (0.1789 mmol) of dmb. One hour later, 23.6 mg (0.0899 mmol) of solid PPh_3 was added, and the solution was stirred for 2 h under N_2(g), during which the color changed to orange. The mixture was then filtered, and the volume of the solution was reduced to about 2 mL in vacuo. Diethyl ether was added to precipitate the product as an orange polycrystalline solid. The product was collected by filtration and washed with diethyl ether. Yield: 16.3 mg (0.0076 mmol), 58%. The compound was identified by X-ray crystallography. ^{1}H NMR (CD_3CN), δ 1.0−2.1 (ppm): (complex, 72H, dmb); 7.3−7.6 (complex, 30H, PPh_3). ^{13}C NMR (CD_3CN), δ (ppm): 23.8, 27.6, 27.7, 29.4, 37.8, 38.0, 46.5, 46.6, 61.2, 61.9, 63.1, 63.7 (dmb); 129.7, 129.7, 131.6, 134.4, 134.5 (PPh_3); 134.8, 135.1 (C≡). ^{31}P NMR (C_6D_6), δ (ppm): 50.5 (^1J(PtP) = 2252 Hz, ^2J(PtP) = 497 Hz, ^3J(PtP) = 148 Hz). ^{195}Pt NMR (CD_2Cl_2), δ (ppm): −2520 (inner ^{195}Pt, fwhm ~20 ppm), −2650 (outer ^{195}Pt, d of t, ^1J(PtP) = 2280 Hz, ^1J(PtPt) = 330 Hz). FT-IR (KBr) 2146 cm^{-1} (ν(N≡C)). FT-Raman (solid): 2169, 2197 cm^{-1} (ν(N≡C)); 162, 84 cm^{-1} (ν(PtPt)). FAB *m*/*z*: calcd for $Pt_4(dmb)_4(PPh_3)_2Cl$ 2101.5, obsd 2100 (relative intensity ~3%); calcd for $Pt_4(dmb)_4Cl$ 1576.9, obsd 1576.1 (relative intensity 100%). UV−vis (ethanol): λ_{max} (ϵ) 405 (35 800), 358 (31 900), 296 nm (22 400 M^{-1} cm^{-1}) at room temperature. X-ray fluorescence confirmed the presence of Pt, P, and Cl in a 2:1:1 ratio. Dark orange crystals suitable for X-ray crystallography were obtained by slow diffusion of *tert*-butyl methyl ether into an acetonitrile solution of the product under N_2(g) atmosphere in the presence of a slight excess of dmb and PPh_3. The presence of acetonitrile and water as solvate molecules was detected by crystallography.

Synthesis of the $\{[Pt_4(dmb)_4(diphos)]Cl_2\}_n$ Polymers. The polymeric materials were prepared in the same way. A typical example is described below.

$\{[Pt_4(dmb)_4(dpph)]Cl_2\}_n$ (4). To a suspension of $Pt_2(dba)_3{\cdot}CHCl_3$ (0.063 g, 0.050 mmol) in 10 mL of acetone was added solid dmb (0.0820 g, 0.631 mmol). This mixture was stirred under N_2 atmosphere for 4 h, during which the black powder ($Pt_2(dba)_3{\cdot}CHCl_3$) slowly dissolved and the solution became yellow-orange. Subsequently, 0.0172 g of dpph (0.037 mmol) was dissolved in 3 mL of CH_2Cl_2, and the solution was added to the yellow-orange solution. The color became deeper and turned red-orange. After being stirred for an additional 2 h, the mixture was filtered, and the filtrate was concentrated to about 6 mL under vaccum. Diethyl ether was then added to precipitate the product, which was recrystallized from acetonitrile/diethyl ether in the presence of dmb. Yield: 0.0537 g, 92%. Anal. Found: C, 45.02; H, 5.52; N, 5.59. Calcd for $\{[Pt_4(dmb)_4(dpph)]Cl_2\}_n$: C, 45.22; H, 5.26; N, 5.41. T_{dec} = 132 °C. ^{1}H NMR (CD_3CN), δ (ppm): 0.9−2.1 (complex, dmb); 2.76 (m, CH_2P); 7.3−7.8 (complex, PhP). ^{31}P NMR (C_6D_6), δ (ppm) 54.5 (^1J(PtP) = 2198 Hz, ^2J(PtP) = 497 Hz). FT-IR (KBr): 2145 cm^{-1} (ν(N≡C)). UV−vis (CH_3CN): λ_{max} 396, 362, 294 nm at room temperature.

Data for $\{[Pt_4(dmb)_4(dppp)]Cl_2\}_n$ (3). Yield: 88%. Anal. Found: C, 44.94; H, 5.69; N, 5.67. Calcd for $\{[Pt_4(dmb)_4(dppp)Cl_2]{\cdot}H_2O{\cdot}CH_3CN\}_n$: C, 44.84; H, 5.29; N, 5.96. T_{dec} = 138 °C. ^{1}H NMR (CD_3CN), δ (ppm): 0.9−2.1 (complex, dmb); 2.60 (m, CH_2P); 7.3−7.8 (complex, PhP). ^{31}P NMR(C_6D_6), δ (ppm): 54.8 (^1J(PtP) = 2185 Hz, ^2J(PtP) = 498 Hz). FT-IR (KBr): 2144 cm^{-1} (ν(N≡C)). UV−vis (CH_3CN): λ_{max} 396, 362, 296 nm at room temperature.

Data for $\{[Pt_4(dmb)_4(dppb)]Cl_2\}_n$ (2). Yield: 91%. Anal. Found: C, 43.56; H, 5.28; N, 5.42. Calcd for $\{[Pt_4(dmb)_4(dppb)]Cl_2{\cdot}3H_2O\}_n$: C, 43.53; H, 5.29; N, 5.34. T_{dec} = 150 °C. ^{1}H NMR (CD_3CN), δ (ppm): 0.9−2.1 (complex, dmb); 2.76 (m, CH_2P); 7.3−7.9 (complex, PhP). ^{31}P NMR (C_6D_6), δ (ppm): 49.6 (^1J(PtP) = 2212 Hz, ^2J(PtP) = 502 Hz). FT-IR (KBr): 2143 cm^{-1} (ν(N≡C)). UV−vis (CH_3CN): λ_{max} 394, 364, 298 nm at room temperature.

X-ray Crystallography. Intensity data were collected at 293 K on an Enraf-Nonius CAD-4 automatic diffractometer using graphite-monochromated Cu Kα radiation. The NRCCAD[8] programs were used for centering, indexing, and data collection. The unit cell dimensions were obtained by a least-squares fit of 24 centered reflections in the range $20° \le 2\theta \le 35°$. During data collection, the intensities of three standard reflections were monitored every 60 min. No significant decay was observed. An absorption correction was applied to the data on the basis of ψ-scan measurements of nine azimutal reflections. The structure was solved by the application of direct methods using the SOLVER program from NRCVAX[9] and refined by least-squares procedures using the SHELXL-97[10] program. The scattering factors were taken from the *International Tables for X-ray Crystallography* (1992), Vol. C, Tables 4.2.6.8 and 6.1.1.4. At convergence, the final discrepancy indices were R_1 = 0.0738, wR_2 = 0.2097, and S = 1.018. The residual positive and negative electron densities in the final maps were 4.923 and −2.544 e/Å^3 and were located in the vicinity of the Pt atoms. The ORTEP[11] diagram was generated from Xtal-GX. The refinement was carried out using several constraints. The SAME/DELU options were used for the disordered dmb atoms, and the FLAT/DELU options were applied for the phenyl rings. The final occupancies for the disordered dmb are 0.475(11)/0.525(11), 0.674(14)/0.326(14), 0.690(12)/0.310(12), and 0.646(12)/0.354(12). Two molecules of acetonitrile and two water molecules were located by a ΔF map in the asymmetric unit.

Instruments. The UV−visible spectra were recorded on a Hewlett-Packard 8452A diode array spectrometer. The chemical analysis measurements were performed at the Université de Montréal for C,H,N. The mass spectra were acquired on a Kratos MS-50 TCTA spectrometer using an Iontech model FAB 11NF saddle-field source operating at 70 kV with 2 mA current. The samples were contained in thiolglycerol or NBA matrixes. The FT-IR (4000−600 cm^{-1}) spectra were obtained on a Bomem (MB-102) spectrometer, and the Raman spectra at 298 K in the solid state were acquired using a Bruker IFS 66/CS FT-IR spectrometer coupled with an FRA 106 FT-Raman module using a Nd:YAG laser (1064 nm excitation) and a Notch filter (cutoff ~50 cm^{-1}). The X-ray powder diffraction patterns were measured with a the Rigaku/USA instrument using a Cu irradiation tube operating at 40 kV and 30 ma. The differential scanning calorimetry experiments were performed using a 5A DSC 7 Perkin-Elmer instrument, and the temperature was

(4) (a) Sykes, A. G.; Mann, K. R. *Inorg. Chem.* **1990**, *29*, 4449. (b) Sykes, A. G.; Mann, K. R. *J. Am. Chem. Soc.* **1988**, *110*, 8252. (c) Fortin, D.; Drouin, M.; Turcotte, M.; Harvey, P. D. *J. Am. Chem. Soc.* **1997**, *119*, 531. (d) Fortin, D.; Drouin, M.; Harvey, P. D. *J. Am. Chem. Soc.* **1998**, *120*, 5351. (e) Perreault, D.; Drouin, M.; Michel, A.; Harvey, P. D. *Inorg. Chem.* **1992**, *31*, 3688. (f) Perreault, D.; Drouin, M.; Michel, A.; Harvey, P. D. *Inorg. Chem.* **1992**, *31*, 2740. (g) Che, C.-M.; Herbstein, F. H.; Schaefer, W. P.; Marsh, R. E.; Gray, H. B. *Inorg. Chem.* **1984**, *23*, 2572. (h) Rhodes, M.; Mann, K. R. *Inorg. Chem.* **1984**, *23*, 2053. (i) Miskowski, V. M.; Rice, S. F.; Gray, H. B.; Dallinger, R. F.; Milder, S. J.; Hill, M. G.; Exstrom, C. L.; Mann, K. R. *Inorg. Chem.* **1994**, *33*, 2799. (j) Che, C.-M.; Wong, W.-T.; Lai, T.-F.; Kwong, H.-L. *J. Chem. Soc., Chem. Commun.* **1989**, 243. (k) Harvey, P. D.; Drouin, M.; Michel, A.; Perreault, D. *J. Chem. Soc., Dalton Trans.* **1993**, 1365. (l) Boyd, D. C.; Matsch, P. A.; Mixa, M. M.; Mann, K. R. *Inorg. Chem.* **1986**, *25*, 3331. (m) Perreault, D.; Drouin, M.; Michel, A.; Harvey, P. D. *Inorg. Chem.* **1993**, *32*, 1903. (n) Sykes, A. G.; Mann, K. R. *J. Am. Chem. Soc.* **1990**, *112*, 7247. (o) Harvey, P. D.; Murtaza, Z. *Inorg. Chem.* **1993**, *32*, 4721. (p) Gladfelter, W. L.; Gray, H. B. *J. Am. Chem. Soc.* **1980**, *102*, 5909.
(5) Maitlis, P. M.; Moseley, K. *J. Chem. Soc., Chem. Commun.* **1971**, 982.
(6) Weber, W. P.; Gokel, G. W.; Ugi, I. K. *Angew. Chem., Int. Ed. Engl.* **1972**, *11*, 530.
(7) (a) Perrin, D. D.; Armarego, W. L. F.; Perrin, D. R. *Purification of Laboratory Chemicals*; Pergamon: Oxford, U.K., 1966. (b) Gordon, A. J.; Ford, R. A. *The Chemist's Companion: A Handbook of Practical Data, Techniques, and References*; Wiley: New York, 1972; p 436.
(8) LePage, Y.; White, P. S.; Gabe, E. J. NRCCAD: An Enhanced CAD-4 Control Program. *Proceedings of the American Crystallographic Meeting*, Hamilton, Canada, 1986; Abstract PA23.
(9) Gabe, E. J.; LePage, Y.; Charland, J.-P.; Lee, F. L.; White, P. S. *J. Appl. Crystallogr.* **1989**, *22*, 384.
(10) Sheldrick, *G. SHELX-97*; University of Göttingen: Göttingen, Germany, 1997.
(11) Johnson, C. K. In *ORTEP in Xtal GX*; Hall, Du-Boulay, Eds.; University of Western Australia: 1995.

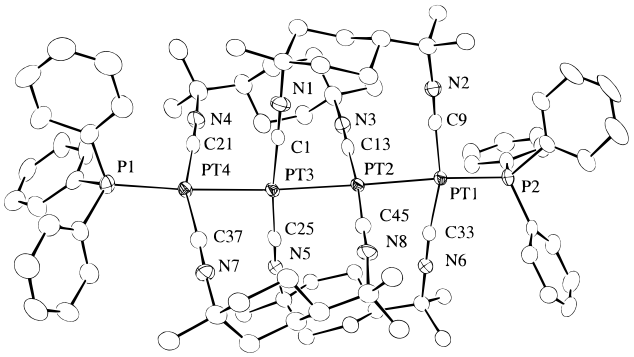

Figure 1. ORTEP drawing for **1**. The ellipsoids represent 50% probability, and the H atoms, Cl^- ions, and solvate molecules are omitted for clarity.

controlled using both an N_2(l) and a 5B TAC 7/DS thermal analysis controller. The temperature calibration was done with indium and water samples. The precision for the temperature was ±0.1 °C, and that for the calorimetric measurements was ±0.1%. Typically, each sample weighed from 5 to 10 mg and the scan rate was 10.0 °C/min. The DSC cells were two independent dual furnaces constructed of platinum−indium alloy with platinum resistance heaters and temperature sensors. The luminescent spectra (excitation and emission) were acquired on a steady-state LS-100 spectrofluorometer from Photon Technology Inc. or on a Fluorolog II instrument from Spex. The emission lifetimes were measured using a single-photon-counting apparatus equipped with an N_2 flash lamp pulsing at 10 kHz.

Calculational Details. All of the MO calculations were of the extended Hückel type (EMHO)[12,13] using a modified version of the Wolfsberg−Helmohlz formula.[14] The atomic parameters used for C,[13] N,[13] H,[13] P,[15a] and Pt[15b] were from the literature. Because of limitations in the size of the molecules handled by the program, dmb was replaced by two CH_3NC molecules and PPh_3 was replaced by PH_3. Hence the computed ion is $Pt_4(CNCM_3)_8(PH_3)_2^{2+}$. This methodology is a standard one.[16] The bond distances are those reported for the X-ray structure (averaged values). For **1**, $d(Pt_2) = 2.66$, $d(Pt-P) = 2.33$, $d(P-C) = 1.932$, $d(C\equiv N) = 1.16$, and $d(N-C) = 1.46$ Å. All angles were 90 or 180° for an idealized structure in the first series of calculations. Then other angles were investigated. The detailed description of the graphic programs used in this work can be found in ref 17.

Spin−Lattice Relaxation Times (T_1). The T_1's were measured by the inversion recovery pulse technique. The measurements were performed on a Bruker AC-F 300 NMR spectrometer operating at 75.47 MHz for carbon-13. The temperature was ~21 °C, and the sampling was done over a 20 000 Hz sweep width using 8192 data points to describe the FID's. The solutions of the polymers were saturated in all cases in order to improve the signal-to-noise ratio. The uncertainties are ~5% on T_1.

Results and Discussion

1. Preparation and X-ray Structure for 1. The $d^{10}-d^{10}$ $Pt_2(dba)_3\cdot CHCl_3$ dimer reacts with an excess of dmb and PPh_3 in acetone under inert atmosphere to give the corresponding complex $[Pt_4(dmb)_4(PPh_3)_2]Cl_2$ (**1**) as identified by X-ray crystallography (Figure 1 and Chart 1). In solutions, the cluster is readily air-sensitive, while in the solid state, the complex is relatively stable. Reactions between $Pt_2(dba)_3\cdot C_6H_6$ and dmb (excess) provide yellow luminescent solids which proved too unstable in both the presence and the absence of oxygen for characterization. By addition of PPh_3 to these reactions, similar products were obtained with improved stability, but no crystal suitable for X-ray crystallography was obtained. Finally, the presence of a chlorocarbon, either from the starting $Pt_2(dba)_3\cdot CHCl_3$ material or from added CH_2Cl_2, provides the oxidized orange salts (**1**). The presence of Cl^- ions has been confirmed by X-ray fluorescence, X-ray crystallography (Tables 1 and 2), and mass FAB analysis.

Chart 1

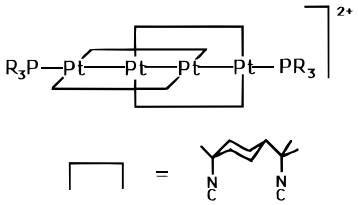

Table 1. Crystallographic Data for **1**

formula $[Pt_4(C_{12}H_{18}N_2)_4(P(C_6H_5)_3)_2]Cl_2\cdot 2H_2O\cdot 2CH_3CN$	fw 2254.25
$a = 12.624(4)$ Å	space group $P1$
$b = 14.24(2)$ Å	$T = -80$ °C
$c = 27.312(3)$ Å	$\lambda = 1.541\ 84$ Å
$\alpha = 92.35(3)°$	$\rho_{calcd} = 1.528$ g cm^{-3}
$\beta = 91.655(15)°$	$\mu = 1.1592$ cm^{-1}
$\gamma = 90.28(5)°$	$R_1{}^a = 0.0738$
$V = 4903(7)$ Å	$wR_2{}^a = 0.2097$
$Z = 2$	

[a] $R_1 = \sum||F_o| - |F_c||/\sum|F_o|$, $wR_2 = \{\sum[w(F_o^2 - F_c^2)^2]/\sum w(F_o^2)^2\}^{1/2}$ $[w = 1/(\sigma^2(F_o^2) + (0.1P)^2)$ where $P = (F_o^2 + 2F_c^2)/3]$.

Table 2. Selected Bond Distances (Å) and Angles (deg) for **1**

	data	av values
d(PtP)	2.328(3), 2.342(3)	2.335
$d(PtPt)_{outer}$	2.654(2), 2.666(2)	2.660
$d(PtPt)_{inner}$	2.641(2)	2.641
$d(PtC)_{outer}$	1.926(9), 1.949(9), 1.955(10), 1.928(9)	1.940
$d(PtC)_{inner}$	1.914(9), 1.915(9), 1.934(10), 1.935(10)	1.925
$\angle PPt_2$	171.13(6), 174.84(7)	173.9
$\angle Pt_3$	175.77(2), 174.83(2)	175.3
$\angle CPtC_{outer}$	163.4(4), 160.1(4)	161.8
$\angle CPtC_{inner}$	175.3(3), 172.7(3)	174.0

The structure exhibits a quasi-linear $P-Pt_4-P$ frame (average $\angle PPt_2$ and $\angle Pt_3$ are 173.9(2.8) and 175.3(5)°, respectively, where the Pt_2 (2.655(2) and 2.666(3) Å, outer; 2.641(2) Å, inner) and PtP distances (average d(PtP) = 2.335(7) Å) indicate the presence of formal single bonds. The comparison of the $d(Pt_2)$ data for the literature Pt_4 complexes shows a clear trend between Pt_2 bond order (BO) and $d(Pt_2)$.[1] The average $d(Pt_2)_{outer}$ and $d(Pt_2)_{inner}$ are 2.98 and 3.20 Å, 2.84 and 2.88 Å, 2.79 and 2.88 Å, 2.75 and 2.73 Å, and 2.70 and 2.71 Å for the Pt_4 species with BO of 0.00, 0.14, 0.25, 0.37, and 0.50, respectively. For **1**, $d(Pt_2)_{outer} = 2.66$ and $d(Pt_2)_{inner} = 2.64$ Å, and these data fall slightly under those for $[Pt_4(NH_3)_8(C_4H_6ON)]_2^{6+}$ (2.70 and 2.71 Å),[1n] for which BO is also 0.50. This small difference is associated with the very different ligand environments of the two complexes. These distances are also somewhat greater than that reported for the closely related linear $[Pt_3(2,6\text{-}Me_2C_6H_3\text{-}NC)_6(PPh_3)_2]^{2+}$ trimer (2.6389(7) Å).[1t] The most interesting feature is the dmb bridging mode where two "$M_2(dmb)_2$" units are depicted forming 20-membered rings, usually encountered for most binuclear species.[4] However a catenate structure is

(12) Hoffmann, R.; Lipscomb, W. N. *J. Chem. Phys.* **1962**, *36*, 2179.
(13) (a) Hoffmann, R.; Lipscomb, W. *J. Chem. Phys.* **1962**, *36*, 2872. (b) Hoffmann, R. *J. Chem. Phys.* **1963**, *39*, 1397.
(14) Ammeter, J. H.; Burgi, H. B.; Thibeault, J. C.; Hoffmann, R. *J. Am. Chem. Soc.* **1978**, *100*, 3686.
(15) (a) Tatsumi, K.; Hoffmann, R.; Yamamoto, A.; Stille, J. K. *Bull. Chem. Soc. Jpn.* **1981**, *54*, 1857. (b) Macchi, P.; Proserpio, D. M.; Sironi, A. *Organometallics* **1997**, *16*, 2101.
(16) Mealli, C. *J. Am. Chem. Soc.* **1985**, *107*, 2245.
(17) Mealli, C.; Proserpio, D. M. *J. Chem. Educ.* **1990**, *67*, 399.

Table 3. Comparison of the Spectroscopic and Structural Data for Linear Pt_3 and Pt_4 Complexes

complex	assignt method[a]	ν(M−M)/cm^{-1}	d(M−M)/Å	ref
$Pt_4(dmb)_4(PPh_3)_2^{2+}$ (**1**)	rel int + comp	162 (a_1) 84 (a_1)	2.655(2), 2.641(2) 2.666(2)	this work
$Pt_4(NH_3)_8(C_5H_4NO)_4^{5+}$	RR	149 (a_{1g}) 69 (a_{1g})	2.774 2.877	*b*, 1p, 1g, 1r
$Pt_4(NH_3)_8(C_5H_5N_2O_2)_4^{5+}$	RR	149 (a_{1g}) 67 (a_{1g})	2.793, 2.865 2.810	*b*, 1d
$Pt_4(en)_4(C_5H_4NO)_4^{5+}$	RR	133 (a_{1g}) 67 (a_{1g})	2.830, 2.830 2.906	*b*, 1d, 1g
$Pt_3(popop)_4^{6+}$	RR	147 (IR) 85 (R)	2.925	*c*, *d*

[a] RR = resonance Raman. Rel int + comp = assignments based upon the high intensity of $\nu(Pt_2)$ and comparison of data for well-established compounds such as these included here. [b] Stein, P.; Mahtani, H. K. *J. Am. Chem. Soc.* **1991**, *111*, 3491. [c] Dickson, M. K.; Fordyce, W. A.; Appel, D. M.; Alexander, K.; Stein, P.; Roundhill, D. M. *Inorg. Chem.* **1982**, *21*, 3858. Marsh, R. E.; Herbstein, F. H. *Acta Crystallogr., Sect. B* **1983**, *39*, 280. [d] Stein, P.; Dickson, M. K.; Roundhill, D. M. *J. Am. Chem. Soc.* **1983**, *105*, 3489.

observed where two dmb ligands bridge the first and third Pt metals, while the two others bind the second and fourth. To our knowledge this example is unique in dmb chemistry. The dmb bite distances (5.321(4) and 5.307(4) Å) are the longest ones ever reported.[4] The closest reported values for this distance are 5.284(2) and 5.28(2) Å for the "windmill" $[Ir_2Ag(dmb)_4(L)_2](PF_6)_3$ complexes (L = PPh_3, DMSO),[4a,b] in which the Ag^+ cation is encapsulated inside the "$Ir_2(dmb)_4$" frame. The recently reported $\{[Ag(dmb)_2]Y\}_n$ polymers (Y = PF_6^-, BF_4^-, NO_3^-, ClO_4^-, $CH_3CO_2^-$, $TCNQ^-$)[4c−e] also exhibit long dmb bite distances ranging from 4.95 to 5.19 Å. The difference is that no encapsulation occurs within the polymers. The d(PtC) data are normal and compare favorably to those known for $Pt_3(CN\text{-}t\text{-}Bu)_6$ (1.901 Å, terminal; 2.085 Å, bridging)[18] and $Pt(CN\text{-}t\text{-}Bu)Cl_2(\mu\text{-}CN)Pt(CN\text{-}t\text{-}Bu)_2Cl\cdots Pt(CN\text{-}t\text{-}Bu)_2Cl_2$ (1.93 Å).[19] Finally, the dihedral angle between the $M_2(CN)_4$ planes is not 90°, but 74.7° (local symmetry for $M_4(CN)_8$ is D_2). This angle is very likely associated with van der Waals interactions between the adjacent dmb's and with crystal packing.

2. NMR Spectra for 1. A number of particularities have been noticed.

First, the ^{1}H NMR spectra exhibit very complex dmb signals spreading over 1 ppm. Crystallography indicates disorder within the dmb ligand (Experimental Section), and theoretically five geometric and two optical isomers are predicted (Supporting Information). The complex ^{1}H NMR behavior does not occur in binuclear compounds of the type "$M_2(dmb)_2$" where the dmb ligands are placed trans to each other.[4e,m] On the other hand, this head-to-tail chemistry was previously reported for "windmill" $M_2(dmb)_4$ compounds,[4a] where four geometric isomers are possible. This complexity is associated with the relative proximity of the dmb's placed cis to each other, inducing greater chemical shift differences (when compared to a trans geometry), and with the fact that two types of Pt nuclei are present (inner and outer).

Second, the ^{31}P NMR spectra exhibit the expected coupling patterns based upon the natural abundance (33.7%) of the ^{195}Pt nuclei (10 possible isotopomers). The ^1J(PtP) and ^2J(PtP) values (2250 and 498 Hz) are respectively the smallest and largest values ever reported for low-valent Pt clusters.[20−25] This comparison includes butterfly and tetrahedral Pt complexes, triangular Pt_3 complexes, and the $Pt_2(dppm)_3$ dimer and mainly reflects the difference between cyclic and linear clusters (Supporting Information).

3. Raman Spectra for 1. The $\nu(M_2)$ data were extracted from Raman spectroscopy to address the amplitude of the M_2 interactions. The strategy of the assignment is based upon the comparison with literature data for closely related linear Pt_n clusters (for which $\nu(M_2)$ has been confirmed by resonance Raman spectroscopy), also taking into account the M_2 bond lengths or separations and the commonly encountered high intensity of the $\nu(M_2)$ modes. Resonance Raman spectroscopy could not be used in this work because the samples proved to be extremely laser sensitive. The two totally symmetric $\nu(M_2)$ modes are readily observed at 162 and 84 cm^{-1}, as only these two features are present in this region. The favorable comparison of these two frequencies with the literature values for well-established compounds indeed supports the assignments (Table 3). Using empirical equations relating $d(Pt_2)$ with $F(Pt_2)$, the metal−metal force constant (in mdyn Å^{-1}),[26] and the average $d(Pt_2)$ data (2.66 Å), eq 1 computes $F(Pt_2)$ = 2.36 mdyn Å^{-1}, which is normal for Pt−Pt single bonds (see literature comparisons in ref 19).

$$d(Pt_2) = -0.233 \ln F(Pt_2) + 2.86 \qquad (1)$$

4. Preparation and Characterization of 2−4. These polymers are prepared in the same way as **1** and are obtained in good yields. The identity of the compounds is readily confirmed spectroscopically by comparison with **1**. According to the X-ray diffraction patterns, these materials are amorphous. On the basis of the Pt_4^{2+} geometry, the diphos ligands can only induce the formation of a polymeric structure (Chart 2). Evidence is available to demonstrate the polymeric nature of these materials, rather than oligomeric. First, for dppb materials (for instance $\{Pt_4(dmb)_4(dppb)^{2+}\}_n$), for n = 1 the ratio of the ^{1}H NMR signals ^{1}H phenyl/^{1}H dmb is theoretically 40/76 (0.53). For $n \rightarrow \infty$, this ratio decreases to 20/76 (0.26). Experimentally we obtain ~0.25 for all three polymers. Second, there is no evidence

(18) Green, M.; Howard, J. A.; Spencer, J. L.; Stone, G. F. *J. Chem. Soc., Chem. Commun.* **1975**, 3.
(19) Harvey, P. D.; Truong, K. D.; Aye, K. T.; Drouin, M.; Bandrauk, A. D. *Inorg. Chem.* **1994**, *33*, 2347.
(20) Moor, A.; Pregosin, P. S.; Venanzi, L. M.; Welch, A. J. *Inorg. Chim. Acta* **1984**, *85*, 103.
(21) Douglas, G.; Manojlovic-Muir, L.; Muir, K. W.; Jennings, M. C.; Lloyd, B. R.; Rashidi, M.; Schoettel, G.; Puddephatt, R. J. *Organometallics* **1991**, *10*, 3927.
(22) Hao, L.; Vittal, J. J.; Puddephatt, R. J.; Manojlovic-Muir, L.; Muir, K. W. *J. Chem. Soc., Chem. Commun.* **1995**, 2381.
(23) Dahmen, K.-H.; Imhof, D.; Venanzi, L. M. *Helv. Chim. Acta* **1994**, *77*, 1029.
(24) Ferguson, G.; Lloyd, B. R.; Puddephatt, R. J. *Organometallics* **1986**, *5*, 344.
(25) Manojlovic-Muir, L.; Muir, K. W.; Grossel, M. C.; Brown, M. P.; Nelson, C. D.; Yavari, A.; Kallas, E.; Moulding, R. P.; Seddon, K. R. *J. Chem. Soc., Dalton Trans.* **1986**, 1955.
(26) Harvey, P. D. *Coord. Chem. Rev.* **1996**, *153*, 175 and references cited therein.

Chart 2

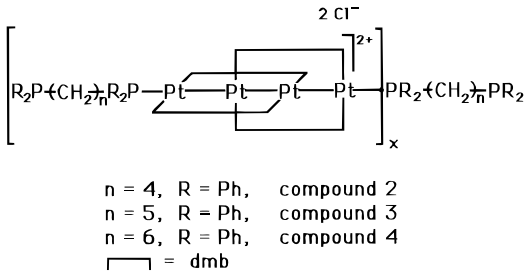

for free ^{31}P in the NMR spectra, which is consistent with the very low concentration of end groups. Further evidence is provided from ^{13}C NMR spin−lattice T_1 measurements and viscometry. In our previous work on the $\{[M(dmb)_2]Y\}_n$ polymers (M = Cu, Ag) (see ref 4c, footnote 32), it has been possible to demonstrate the oligomeric nature of some of the materials using T_1 of the quaternary ^{13}C located beside the CH_3 group in dmb. The ^{13}C signal occurs at ∼63 ppm in CD_3CN. The observed rate of relaxation is given by the rate of relaxation due to dipole−dipole interactions, $(T_1^{DD})^{-1}$, plus a series of rates due to other processes. Because of the very close similarities in structure between the polymers (where only the counteranions or the central metal atoms were varied), the rates for the other processes are assumed to be essentially constant from one material to the other, leaving only T_1^{DD} as the main variable. The latter is inversely proportional to τ_c (the correlation time), which is related to the volume of the tumbling molecule. Hence, the smaller τ_c is, the greater is the molecular weight of the material. This approximation is crude but is in the right direction. To test this hypothesis, the dimeric $Ag_2(dmb)_2(NO_3)_2$ is compared to **1**−**4**. The T_1 data for the ^{13}C NMR signal at 63 ppm are 7.26 s for $Ag_2(dmb)_2(NO_3)_2$, 3.76 s for **1**, and 1.69−2.24 (±0.01) s for **2**−**4** and are indeed consistent with these predictions.

For the viscosity measurements, the standard equation relating the intrinsic viscosity, $[\eta]$, and MW (molecular weight) is used:[27]

$$[\eta] = K(MW_n)^a \qquad (2)$$

where K and a are constants related to the nature of the polymer and solvent. Due to the novelty of the materials, the known and related $\{[Cu(dmb)_2BF_4\}_n$ semicrystalline polymer (MW = 156 000 from light diffusion;[4c] MW_n = 133 000 from osmometry (unpublished result)) is used to extract K, and a is set at 0.65 (an average value between 0.5 and 0.8, the two extreme limits observed in the literature).[27] In this case, $[\eta] = 3.08$ cm^3 g^{-1} and K is evaluated to be 1.30×10^{-3}. The $[\eta]$ data for compounds **2**−**4** are given in Table 4, and the estimated MW_n's range from ∼84 000 (∼40 units) to ∼307 000 (∼150 units). Clearly, these materials are polymeric, not oligomeric as was the case for the $\{[Ag(dmb)_2]Y\}_n$ polymers (MW ≤ 10 000).[4c] It is anticipated that the number of CH_2 groups in the diphos controls the local conformations and therefore controls the overall geometry, thereby controlling the relative solubility of the polymers. Further, the quantity of residual phosphine oxides also plays an important role in adding end groups to the system. No attempt was made to vary these polymeric dimensions at this time. It is interesting to note that there is a correlation between $[\eta]$ and T_1 where $[\eta]$ is greater T_1 is shorter (Table 4).

Table 4. Comparison of $[\eta]$ with T_1 NMR Data

compd	$[\eta]^a$ cm^3 g^{-1}	$MW_n{}^b$	units	T_1 ^{13}C NMR peak at 63 ppm/s
1		∼2 000	1	3.76
2	3.66	∼203 000	∼100	2.19
3	4.78	∼307 000	∼150	1.69
4	2.06	∼84 000	∼40	2.24

[a] $[\eta]$ is the intercept value extracted from the graph $[(\eta_{solutions} - \eta_{solvent})/\eta_{solvent}]$/conc vs conc, with conc given in g/mL. [b] MW_n = number-average molecular weight. It is calculated using eq 2, with a = 0.65 and $K = 1.30 \times 10^{-3}$ as extracted from the standard polymer semicrystalline $\{[Cu(dmb)_2]BF_4\}_n$ (MW_n = 133 000 from osmometry). The data are approximations and are used only to provide an order of magnitude to the molecular dimensions.

In the solid state, there is no phase transition between room and decomposition temperatures (∼132−150 °C). The result also contrasts with those for the $\{[M(dmb)_2]Y\}_n$ materials (M = Cu, Ag),[4c] where glass transitions were observed in the 35−90 °C range.

Finally, on the basis of ^1H NMR, IR, and chemical analysis, evidence for H_2O and CH_3CN crystallization molecules is also found, even upon leaving the samples to dry under an N_2 flow or under vaccum. This result is in agreement with the X-ray data for **1**, where two H_2O and two CH_3CN molecules per Pt_4^{2+} unit are found in the crystal lattice. The best formulation is $\{[Pt_4(dmb)_4(diphos)]Cl_2 \cdot xH_2O \cdot yCH_3CN\}_n$.

5. MO Computations. This section addresses the MO picture of the Pt_4 cluster qualitatively since it is the first of its kind, where the intermetallic distances are the shortest and the M formal oxidation state is the lowest in the Pt_4 series. Relevant to this work, one should refer to ref 28, Chapter 13.2, notably the description of the related linear chain $Pt(CN)_4^{x-}$ species, and Chapter 18.2, for the description of the ML_3 fragment[29] and the singly bonded $Pd_2(dmb)_2X_2$ complexes (X = Cl, Br, I),[29] including the effect of the PdL_3-PdL_3 twist angle on the MO diagram. In the latter cases, the M_2 σ-bonding arises from three square planar $ML_3^\bullet$ fragments (i.e., $^\bullet Pd(CNR)_2X$) interacting side-by-side. These interactions generate the $d\delta/d\delta^*$ and $d\sigma/d\sigma^*$ MO's. However, due to symmetry, these MO's are bound to mix greatly. In addition, the HOMO and LUMO exhibit atomic contributions involving the M s and p_z orbitals, as well as some orbitals provided by the various ligands. The present computational results are consistent with previous findings which are now described.

For **1**, the model complex $Pt_4(CNCH_3)_8(PH_3)_2^{2+}$ (**5**) is used and can best be described by the interactions of the fragments $PtL_2(PH_3)^+ \cdots PtL_2 \cdots PtL_2 \cdots PtL_2(PH_3)^+$ (L = CH_3NC). The first calculations deal with the geometry where the twist angle is set at 90°. The $^\bullet PtL_2(PH_3)^+$ fragment (C_{2v} local symmetry) is isolobal with $AuPR_3$, $Mn(CO)_5$, H, and CH_3, which possess a frontier orbital of a_1 symmetry. This a_1 orbital is essentially a dp hybrid which bulges outside of the planar T-shaped Pt fragment, and its atomic contribution is as follows: 16% d_{z^2}, 36% $d_{x^2-y^2}$, 12% p_x, and 18% s Pt orbitals (the x axis is parallel to the missing vertex of the Pt square planar coordination). Below this orbital lie the remaining four d M atomic orbitals. The interaction of this fragment with a linear Pt^0L_2 complex (L = $CNCH_3$) generates a new fragment $[H_3PPtL_2-PtL_2^\bullet]^+$, which is also isolobal with that described above (also C_{2v} local symmetry). The MO scheme for this fragment is almost entirely

(27) Margerison, D.; East, G. C. *Introduction to Polymer Chemistry*, 1st ed.; Pergamon Press Ltd.: London, 1967.

(28) Albright, T. A.; Burdett, J. K.; Whangbo, M.-H. *Orbital Interactions in Chemistry*; Wiley: New York, 1985.

(29) (a) Gilmour, B. I.; Mingos, D. M. P. *J. Organomet. Chem.* **1986**, *302*, 127. (b) Harvey, P. D.; Murtaza, Z. *Inorg. Chem.* **1993**, *32*, 4721.

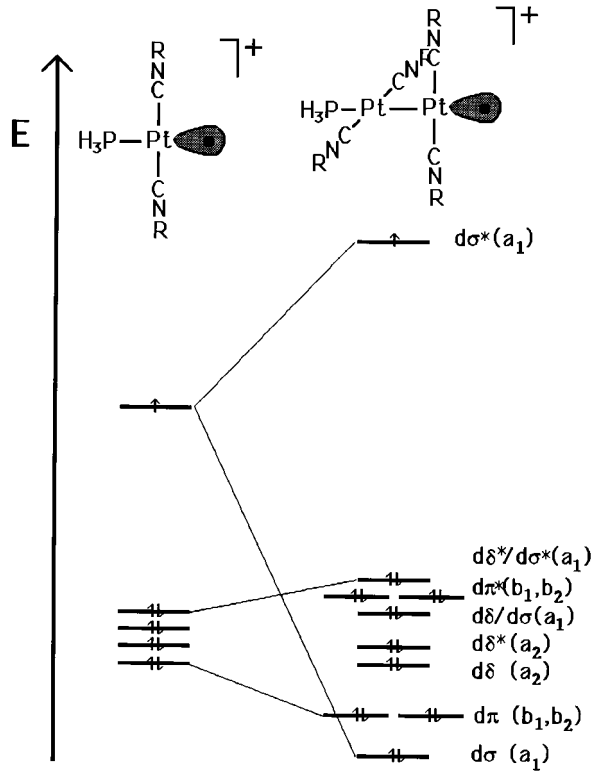

Figure 2. MO correlation diagram for the $[^{\bullet}Pt(CNR)_2(PH_3)]^+$ and $[^{\bullet}Pt_2(CNR)_4(PH_3)]^+$ fragments.

dominated by the Pt−Pt bonding. A qualitative correlation diagram between $^{\bullet}PtL_2(PH_3)^+$ and $^{\bullet}PtL_2-PtL_2(PH_3)^+$ is provided in Figure 2. The singly occupied a_1 frontier orbital which arises from a dσ* MO of the binuclear fragment also exhibits this dp hybrid, pointing toward the missing vertex of the square planar Pt coordination. One important difference from the literature (generally using phosphine ligands)[27,28] is that this frontier orbital is heavily mixed with the π-system of the CNR ligands. For the lower energy MO's (see the series dδ*/dσ* down to dσ in Figure 2), no or very little mixing with the π-system of the CNR ligands occurs.

Subsequently, the interactions between two $^{\bullet}PtL_2-PtL_2(PH_3)^+$ fragments generate the model complex **5**. In the absence of a relativistic correction for Pt, the overall computational results should be considered as an approximation. The main features are as follows: (1) the HOMO is a filled dσ* involving $d_{x^2-y^2}$, d_{z^2}, s, and p_x M orbitals (x still being the Pt_4 molecular axis), (2) as predicted, four dπ/dπ*, four dδ/dδ*, and two dσ/dσ* MO's are observed, (3) the HOMO−1 to HOMO−18 (which are all essentially M centered) are closely located (to within 1.6 eV), and (4) numerous dσ, dσ*, dδ, and dδ* MO's are greatly mixed in nature. This EHMO model places four quasi-degenerated π*(CNR) MO's as LUMO+1 to LUMO+4 and the expected empty dσ* as the LUMO. The latter lies just ∼0.06 eV below the π*(CNR)'s. Since EHMO is a qualitative method, such a small difference is not significant in addressing the correct relative MO energies. In this case, one should address the problem experimentally (see section below).

The last series of computations deals with the MO description with the change in twist angle. The total EHMO energy plotted against the dihedral angle between 90° (local symmetry = D_{2d}) and 30° (local symmetry = D_2) for **5** shows an increase of 0.96 eV in that range. However, this total energy is practically flat (within ∼0.03 eV) between 90 and 70°. A close examination of the individual MO energies and atomic contributions between these twist angles shows practically *no* change in comparison with that reported in Table 5. This is, of course, due to the cylindric symmetry of the Pt−Pt single bond. At higher angles, the total energy increases more rapidly with the twist angle and relates the change in dπ and dδ contacts. At angles approaching 40−30°, $CH_3\cdots CH_3$ interactions increase and induce a rapid increase in total energies. On the basis of literature results, twist angles are generally found between 74 and 81° for linear Pt_n− and Pd_n−CNR complexes (74.7° in **1**, 74.5° in $[Pd_3(CNMe)_6(PPh_3)_2](PF_6)_2$,[30] and 81° in $[Pt_3(2,6\text{-}Me_2C_6H_3NC)_6(PPh_3)_2](PF_6)_2$[1t]).

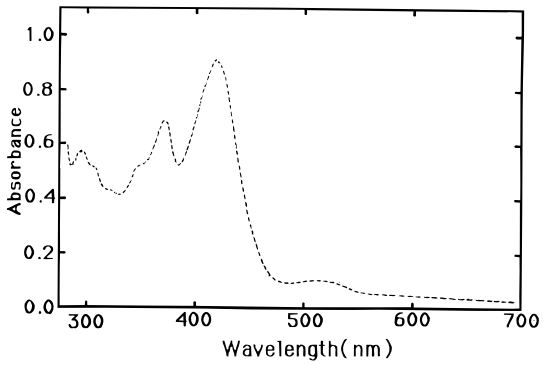

Figure 3. UV−vis spectrum of **1** in EtOH at 77 K.

Table 5. Spectroscopic Data for **1**

T/K	λ_{max}/nm	λ_{max}/cm^{-1}	fwhm/cm^{-1}	ϵ/M^{-1} cm^{-1}	assignt
298	405	24 700	1820	35 800	^{1}(dσ* → dσ*)
77	412	24 300	1580		
298	523	19 100	1330	3 300	^{3}(dσ* → dσ*)
77	515	19 400	1100		

6. Electronic Spectra. The electronic spectra are characterized by strong narrow absorptions in the visible region (Figure 3) and have some similarities with the absorption spectra of other M−M bonded quasi-linear trimers.[31] In an attempt to provide a reliable assignment for these low-energy electronic bands, one should consider the ϵ data, shapes, and behavior with temperature. Absorption bands arising from dσ → dσ* transitions in M_2 σ-bonded compounds or from dσ* → pσ transitions in M_2 face-to-face and non-M_2-bonded dimers generally undergo a significant decrease in fwhm at lower temperatures. Numerous examples for this phenomena are available in the literature (see examples for d^7-d^7 and d^9-d^9 σ-bonded M_2[29−32] and for non-M_2-bonded dimers such as the d^8-d^8 and $d^{10}-d^{10}$ compounds[33,34]). This change in fwhm is associated with the presence of low-frequency Franck−Condon active vibrational modes, which upon warming, allows the population of vibrationnally excited levels in the ground state to give rise to "hot bands" in the spectra according to a Boltzmann distribution. Upon cooling, these levels are less populated and fwhm decreases. Such modes are generally $\nu(M_2)$ and, on some occasions, ν(ML) if L is heavy or weakly bonded (so ν(ML) is small) and, of course, active in the Franck−Condon term. A good

(30) Balch, A. L.; Boehm, J. R.; Hope, H.; Olmstead, M. M. *J. Am. Chem. Soc.* **1976**, *98*, 7431.
(31) Balch, A. L.; Catalano, V. J.; Chatfield, M. A.; Nagle, J. K.; Olmstead, M. M.; Reedy, P. E., Jr. *J. Am. Chem. Soc.* **1991**, *113*, 1252.
(32) For examples, see: (a) Harvey, P. D.; Johnston, P.; Coville, N. J. *Can. J. Chem.* **1994**, *72*, 2176 and references cited therein. (b) Harvey, P. D.; Butler, I. S.; Barreto, M. C.; Coville, N. J.; Harris, G. H. *Inorg. Chem.* **1988**, *27*, 639 and references cited therein.
(33) Smith, D. M. Ph.D. Dissertation, California Institute of Technology, 1989.
(34) (a) Harvey, P. D.; Gray, H. B. *J. Am. Chem. Soc.* **1988**, *110*, 2145. (b) Piché, D.; Harvey, P. D. *Can. J. Chem.* **1994**, *72*, 705.

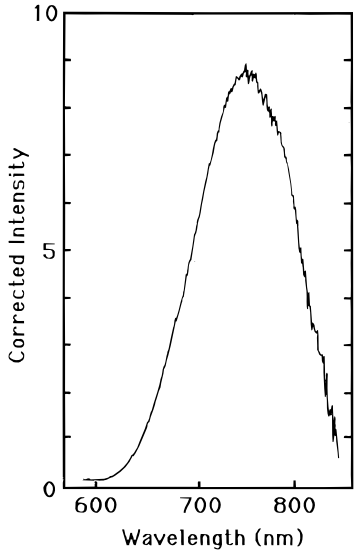

Figure 4. Emission spectrum of **2** in EtOH at 77 K.

description of this phenomena can be found in ref 35. Higher energy modes could be Franck−Condon active, but there would not be significant change in fwhm. For **1**, the fwhm data are summarized in Table 5 and indeed indicate a decrease in fwhm for the lowest energy bands. Furthermore, the bands are so narrow (1100 < fwhm < 1820 cm^{-1}) that only a low-frequency Franck−Condon active mode could explain them. We assign these bands to dσ^* → dσ^* electronic transitions. The low-intensity electronic band (ϵ = 3300 M^{-1} cm^{-1}) located at ∼520 nm for **1** is the singlet−triplet absorption (^{3}(dσ^* → dσ^*)). The singlet−triplet splittings measured at λ_{max} of the absorption bands (∼4900 at 77 K and ∼5600 cm^{-1} at 298 K) are comparable to those of other polynuclear Pt complexes ($Pt_2(POP)_4^{4-}$ (POP═HO(O)POP(O)OH^{2-}), 8800 cm^{-1};[36] $Pt_2(dppm)_3$, 3600 cm^{-1} [34a]). The ϵ value for this band (3300 M^{-1} cm^{-1}, 298 K) also compares favorably to that of $Pt_2(dppm)_3$ (ϵ for ^{3}(pσ ← dδ^*) = 5100, ϵ for ^{3}(pσ ← dσ^*) = 1200 M^{-1} cm^{-1}).[34a] Compounds **2**−**4** exhibit the same spectroscopic signature as that for **1** and the assignments remain.

Compounds **1**−**4** are not luminescent at room temperature, but are at 77 K (Figure 4). In all cases, the structureless emission bands are located around 750 nm and exhibit emission lifetimes ranging from 2.71 to 5.17 ns (Table 6). These relatively long lifetimes and large Stokes shifts (energy difference between the lowest energy allowed electronic absorption and the emission maxima; ∼11 400−12 200 cm^{-1}) indicate that these emissions are phosphorescence. However, the EHMO computations predict at least two candidates for a low-lying emissive excited state: (1) M-centered dσ^* → dσ^* and (2) metal-to-ligand charge transfer (MLCT). For the mononuclear and polymeric materials $[M(CN\text{-}t\text{-}Bu)_4]BF_4$ and $\{[M(dmb)_2]BF_4\}_n$ (M = Cu, Ag), density functional theory indicated that only low-energy MLCT type absorptions and emissions were possible.[4c] A comparative compilation of the Stokes shift data in the latter cases (Supporting Information) shows that these shifts are rather large (26 200−28 700 cm^{-1}).[4c] In the case where only an M-centered emission is possible, i.e., $Ag_2(dmpm)_2^{2+}$ (dmpm = $(Me_2P)_2CH_2$), the Stokes shift is much smaller (11 800 cm^{-1}).[34b] Clearly M-centered excited states (dσ → dσ^*, dσ → pσ^*) provide Stokes shifts that are significantly shorter than that for MLCT. We assign the observed emission bands of compounds **1**−**4** to the ("spin-forbidden") Pt-centered dσ^* → dσ^* electronic transition.

Table 6. Comparison of the Electronic Spectroscopic Data for Compounds **1**−**4**[a]

	λ_{abs}/nm (298 K)	λ_{em}/nm (77 K)	τ_e/ns (77 K)
1	405	750	2.71
2	394	736	4.78
3	394	750	5.15
4	394	755	5.17

[a] Solvent = EtOH.

Acknowledgment. This research was supported by the Natural Sciences and Engineering Research Council of Canada and the Fonds Concertés pour l'Avancement de la Recherche.

Supporting Information Available: A table showing the isotopomer distribution, experimental and simulated ^{31}P NMR and ^{195}Pt NMR spectra for $Pt_4(dmb)_4(PPh_3)_2^{2+}$, a table comparing the NMR data for selected polynuclear Pt complexes, a textual interpretation of the mass FAB spectra, low-resolution mass FAB spectra of $Pt_4(dmb)_4(PPh_3)_2^{2+}$, schematic drawings of the geometric and optical isomers, a table giving a spectroscopic comparison for various low-valent M_n−isocyanide complexes, and an X-ray crystallographic file, in CIF format, for the structure determination. This material is available free of charge on the Internet at http://pubs.acs.org.

IC9807947

(35) Miskowski, V. M.; Smith, T. P.; Loehr, T. M.; Gray, H. B. *J. Am. Chem. Soc.* **1985**, *107*, 7925 and references cited therein.
(36) Stiegman, A. E.; Rice, S. F.; Gray, H. B.; Miskowski, V. M. *Inorg. Chem.* **1987**, *26*, 1112.